3-D Defect Profile Reconstruction from Magnetic Flux Leakage Signals in Pipeline Inspection Using a Hybrid Inversion Method

Junjie Chen

Electric Power Planning & Engineering Institute, Beijing, 100120, China
jjchen@eppei.com

Abstract ─ In this paper, we propose a hybrid inversion approach to reconstruct the profile of arbitrary three-dimensional (3-D) defect from magnetic flux leakage (MFL) signals in pipeline inspection. The region of pipe wall immediately around the defect is represented by an array of partial cylinder cells, and a reduced forward FE model is developed to predict MFL signals for any given defect. The neural network (NN) method is used at first to give a coarse prediction of the defect profile, and the prediction is then utilized as one original solution of the genetic algorithm (GA) to search for the global optimum estimate of the defect profile. To demonstrate the accuracy and efficiency of the proposed inversion technique, we reconstruct defects from both simulated and experimental MFL signals. In both cases, reconstruction results indicate that the hybrid inversion method is rather effective in view of both efficiency and accuracy.

Index Terms ─ Defect reconstruction, genetic algorithm, magnetic flux leakage, neural network, pipeline inspection.

I. INTRODUCTION

Magnetic flux leakage (MFL) inspection is widely used for detecting corrosion defects in pipelines for oil and gas [1]. The inspection devices, referred as in-line-inspection (ILI) tools, are designed for autonomous operation in the pipeline. Once defects have been identified, an equally important problem is the assessment of the size or severity of the defect [2].

In the past, inverse MFL problems were solved based on neural networks [3-5], gradient-based optimization methods [6, 7], GA-based optimization methods [8] and other methods [9, 10]. Neural networks are advantageous in cases where rapid inversions are required. However, their main drawback is that they require a large database for training. The performance of neural networks depends on the data used in training and testing. When the test signal is no longer similar to the training data, performance degrades. In contrast, methods embedding the physical model into the MFL signal inversion process do not require a large database. The physical model and the optimization procedure are crucial for these inversion methods. On the issue of convergence, gradient-based optimization often fails to converge to the global optimum in the presence of multiple local optima, since the optimization problem for defect reconstruction from MFL signals is not a unique solution one. The GA-based approach, on the other hand, begins with a large set of initial search points using well-defined probabilistic tools to guide a search towards regions in the search space that are more likely to contain the global optimum. The GA usually begins with a randomly generated set of original solutions, which may take a long time to converge to the global optimum. Therefore, a suitable selection of the initial search points is rather important for the GA-based approach to improve the efficiency.

In this paper, we propose a hybrid method for 3-D defect reconstruction from MFL signals in pipeline inspection. We develop a reduced forward model of pipe in MFL inspection, and combine NN to GA in inversion process by applying the prediction result of NN as one initial solution of GA. Results of defect reconstruction show that the proposed method has outstanding performance for both simulated and real experimental MFL signals.

The organization of this paper is as follows. In Section II, we introduce the reduced forward FE models of pipe and characterization of defect in MFL inspection. In Section III, we summarize the application of NN and GA to 3-D defect inversion. Section IV gives experimental results based on simulated and realistic experimental MFL data, and Section V gives the conclusions.

II. FORWARD MODEL OF MFL INSPECTION

Figure 1 depicts the corresponding magnetic circuit for an ILI tool for pipe inspection. Permanent magnets magnetize the pipe wall to saturation or near saturation flux density, typically in the axial direction. As shown, the magnetic leakage fields from the pipe wall are detected using uniformly-spaced Hall or coil sensors.

Submitted On: January 14, 2016
Accepted On: February 14, 2017

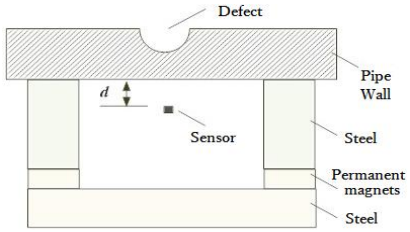

Fig. 1. Simplified magnetic circuit of an ILI tool.

A. Reduced forward model

Based on the magnetic circuit of the ILI tool, we create a 90-degree forward FE model of MFL inspection as shown in Fig. 2 (a), including pipe wall, steel, permanent magnets, air and defect [11, 12]. Compared with the complete 360-degree model, this model could reduce much computation work. Then, a further reduced forward model is proposed as shown in Fig. 2 (b). The reduced forward model only consists of air, nonlinear pipe material and permanent magnets embedded in the pipe wall. The size and distance of permanent magnets could be adjusted so that the simulated MFL signals agree with the real signals.

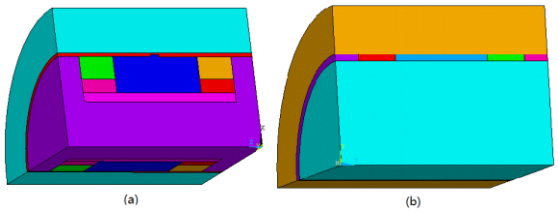

Fig. 2. (a) Basic 90-degree forward model. (b) Reduced forward model.

For the basic forward model and the reduced forward model, the related parameters together with detailed explanations are presented in Table 1, and the Characteristic curves of nonlinear magnetic materials used in the forward model are presented in Fig. 3.

The results of simulation show that, the reduced model only brings less than 5% error while taking one fifth time as the basic model does. Figure 4 shows two samples of MFL images of metal loss defects using the reduced model.

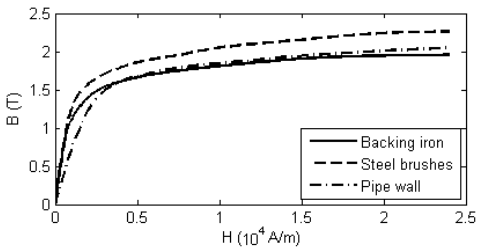

Fig. 3. Characteristic curves of nonlinear magnetic materials used in the forward model.

Table 1: Related parameters for the forward model

Parameter	Value	Unit
Pipe diameter	457	mm
Pipe thickness	14.3	mm
Permanent magnet width	80	mm
Permanent magnet height	30	mm
Brush width	80	mm
Brush height	50	mm
Back height	20	mm
Magnetic pole spacing	1000	mm
Relative permeability	1.26	-
Coercive force	836	KA/m
Lift off value	3	mm

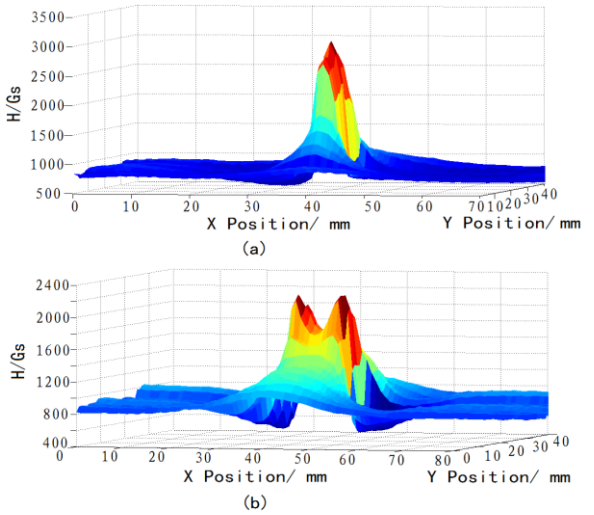

Fig. 4. Simulated MFL images for metal-loss defects using the reduced forward model: (a) internal defect, 100.1 mm×14.3 mm×5.7 mm; (b) external defect, 42.9 mm×42.9 mm×8.6 mm.

B. Defect characterization

The forward computational problem consists of using the reduced FE model to efficiently obtain the magnetic flux field profile for any defect in the pipe. The region of pipe wall immediately around the defect constitutes the 'region of interest' (ROI). To characterize different defect shapes, the radial depth, the tangential width and the axial length of ROI are divided into 7, 10 and 10 parts respectively. Consequently, the ROI could be represented by an array of 7×10×10 partial cylinder cells as illustrated in Fig. 5.

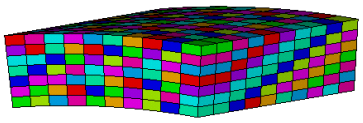

Fig. 5. Defect characterization with 7×10×10 basic model for inversion.

The magnetic conductivity of each cell could be made equal to that of air or iron, resulting in different geometries of the defect. By doing this, any particular defect in the whole defect area could be characterized by a set of 100 depths: $d_1, d_2, ..., d_{100}$, where $\mathrm{di} \in \{0,1,\ldots,7\}$. Thus, the value of a particular depth is encoded as a 3 bit binary string, and the parameter set for the whole defect area can be represented by a 300 bit binary string.

III. INVERSION PROCEDURE USING NN AND GA

In order to take full use of the advantages of both the NN and the GA method, we propose a hybrid method for the defect reconstruction from MFL signals, i.e., to use the results of NN inversion as one initial solution for the GA method.

A. NN prediction

As shown in Fig. 6, a feed-forward NN with a single hidden layer is used to predict the defect profile for the initial solution of GA. The input of the NN consists of feature parameters of MFL signals scanned over the test-pipe, and the output are the parameters of defects corresponding to the MFL signals. The databases of both MFL signals and corresponding defect parameters are separated into training, validation and verification sets.

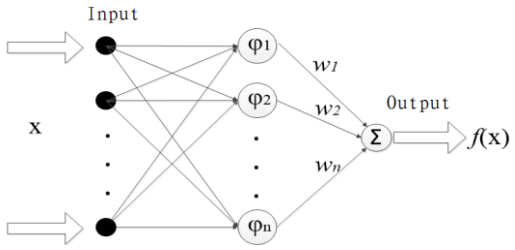

Fig. 6. The feed-forward NN used for prediction.

The training process starts with only one hidden node, and for each training epoch a new node is created. The new input-hidden connections receive random weights and the rest of the weights are obtained by solving (1) with the least square minimization based on the singular value decomposition:

$$A \cdot W_{io} + f_1(A \cdot W_{ih}) \cdot W_{ho} = f_2^{-1}(B), \qquad (1)$$

where A and B represent the input and output training data sets, f_1 and f_2 are nonlinear activation functions for hidden and output nodes, $[W_{ih}]$ the "randomly-fixed" input-hidden weights, and $[W_{io}]$, $[W_{ho}]$ the matrices containing unknown weights, are the input-output and the hidden-output inter-connection weights, respectively.

To generate the training data sets, the reduced forward model shown in Fig. 2 (b) and the defect characterization shown in Fig. 5 were used to get simulated MFL signals. Considering the object for NN inversion result in this paper, only cuboid defects are simulated. Therefore, the trained NN could only provide a cuboid prediction for any arbitrary defect profile as one initial solution.

B. GA inversion process

The flowchart of iterative inversion process using GA for 3-D defect reconstruction is shown in Fig. 7. The inverse problem is solved by minimizing an objective function, representing the difference between the forward model predicted and the realistic measured MFL signal. When the difference is below a pre-set threshold, the defect profile represents the desired solution. The various issues related with the formulation of the inversion process are described below.

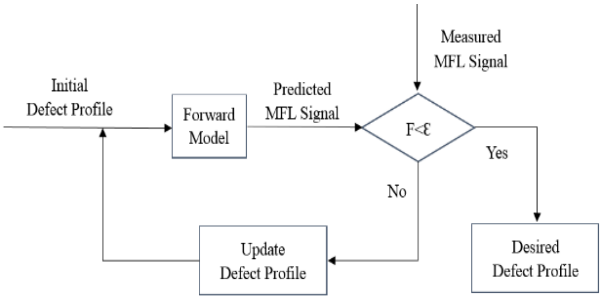

Fig. 7. Iterative inversion flowchart for 3-D defect reconstruction.

As all the three components (radial, tangential and axial) of magnetic flux density carry the information of defect profile, they are all chosen as input signals for the inverse optimization procedure when simulated MFL signals are used. However, only the axial component is used when the inversion is conducted based on realistic measured MFL data, because only the axial component is detected by the ILI tool.

The minimization of an error between measured and predicted MFL signals can be recast as maximizing of the following fitness function:

$$F = \frac{1}{1 + C\sum_{i=1}^{N} \| B_i^m - B_i^{FEM} \|}, \qquad (2)$$

where N is the number of points taken on the signal and C is constant. The global maximum value of F is 1, corresponding to the case the predicted and measured MFL signals are exactly the same. It should also be noted that in case of the error reaching a local minimum other than the global minimum of zero, the relative ratio between the corresponding local and global maximums of F is determined by the constant C.

As shown before, the results of NN inversion is taken as one initial solution for the GA inversion process. This will bring significant help in increasing

both efficiency and possibility for the GA to reach the global optimum solution, which will be presented in Section IV. At the same time, 7 randomly generated original solutions are also used. Furthermore, 2 special 300-bit binary strings, composed of only '0' and only '1' respectively, are added to the initial population for GA in order to keep the diversity of population.

When the original solutions have been selected, a fitness function is used as a measure of closeness of each member in the population to the global optimum solution. Subsequently, a new population is generated by applying genetic operators including reproduction, crossover and mutation on the previous population. The selection mechanism for reproduction favors the highly fit members, so that the members more close to the global optimum are assigned higher probabilities for producing children. Crossover operations ensure that the new population inherits highly fit features, while mutation may add previously unexplored features into the new population. With this, the population drifts to a global or near global solution after a few number of generations in the iterative process.

IV. EXPERIMENTAL RESULTS

In this paper, reconstruction is implemented using biased Roulette-Wheel algorithm with a two-point crossover, and the mutation probability varies between 0.3 and 0.5. The iterative process is terminated when the population of the GA has been updated for 200 times, and at last smoothing is conducted to produce a better defect profile.

Experiments of 3-D defect reconstruction are conducted based on 3-D simulated MFL signals and 1-D measured MFL signals. An internal 100.1 mm× 14.3 mm×5.7 mm cuboid defect (Fig. 8 (a)), an external 42.9 mm×42.9 mm×8.6 mm cuboid defect (Fig. 9 (a)), and an external 42.9 mm×7.15 mm globoid defect (Fig. 10 (a)) are simulated using the reduced forward model. At the same time, the ILI tool is used to measure the axial MFL signals of an 18-inch and 14.3 mm-thick pipe, on which the same defects as the three simulated ones have been artificially made.

The reconstruction is firstly conducted using general GA with initial population composed of 10 randomly generated original solutions. Figure 8 (b), Fig. 9 (b), and Fig. 10 (b) depict the final predicted profiles of the three defects based on 3-D simulated MFL signals. As comparison, Fig. 8 (c), Fig. 9 (c), and Fig. 10 (c) show the predicted defect profiles based on 1-D measured MFL signals. It can be seen that the predicted profiles using 3-D simulated MFL signals match the real defects very well, while at the same time, the inversion results using 1-D measured MFL signals are not so good within a fixed number of iterations. Possible reasons could be lack of enough information carried by the radial and tangential components of magnetic flux density together with error between simulated and realistic MFL signals.

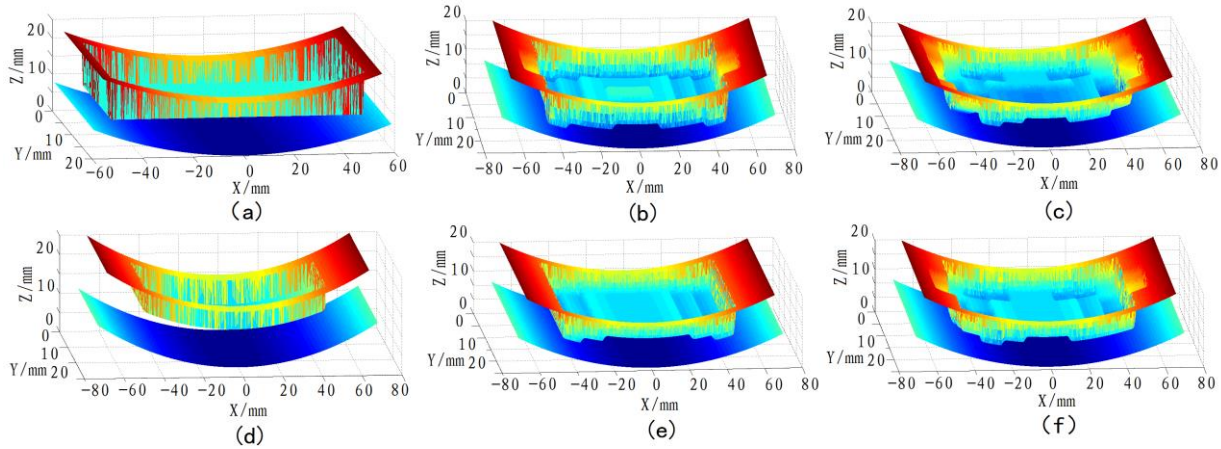

Fig. 8. Reconstruction of internal cuboid defect, 100.1 mm×14.3 mm×5.7 mm: (a) real defect profile; (b), (c) reconstructed defects based on 3-D simulated and 1-D measured signals, using general GA with randomly generated initial population; (d) prediction result of NN inversion; (e), (f) reconstructed defects based on 3-D simulated and 1-D measured signals, using GA with initial solution from NN inversion.

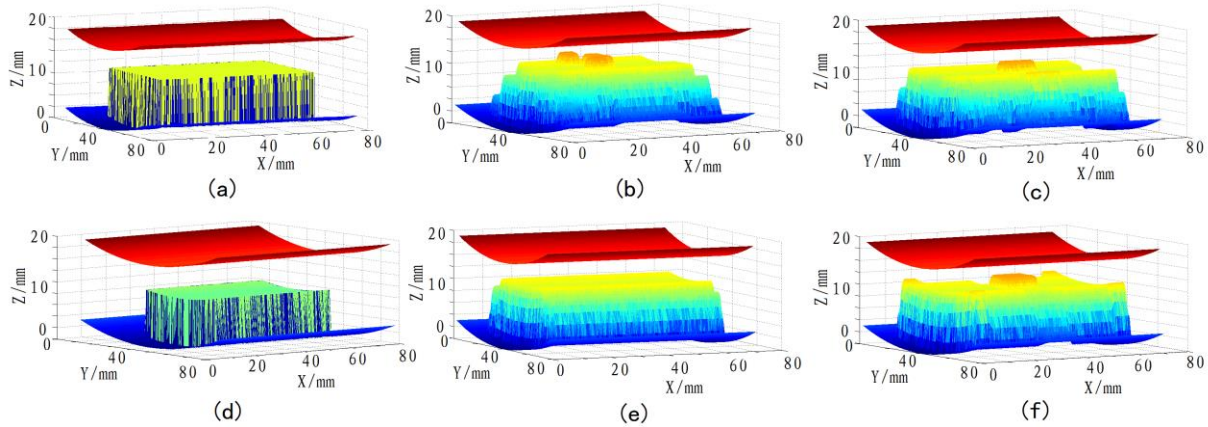

Fig. 9. Reconstruction of external cuboid defect, 42.9 mm×42.9 mm×8.6 mm: (a) real defect profile; (b), (c) reconstructed defects based on 3-D simulated and 1-D measured signals, using general GA with randomly generated initial population; (d) prediction result of NN inversion; (e), (f) reconstructed defects based on 3-D simulated and 1-D measured signals, using GA with initial solution from NN inversion.

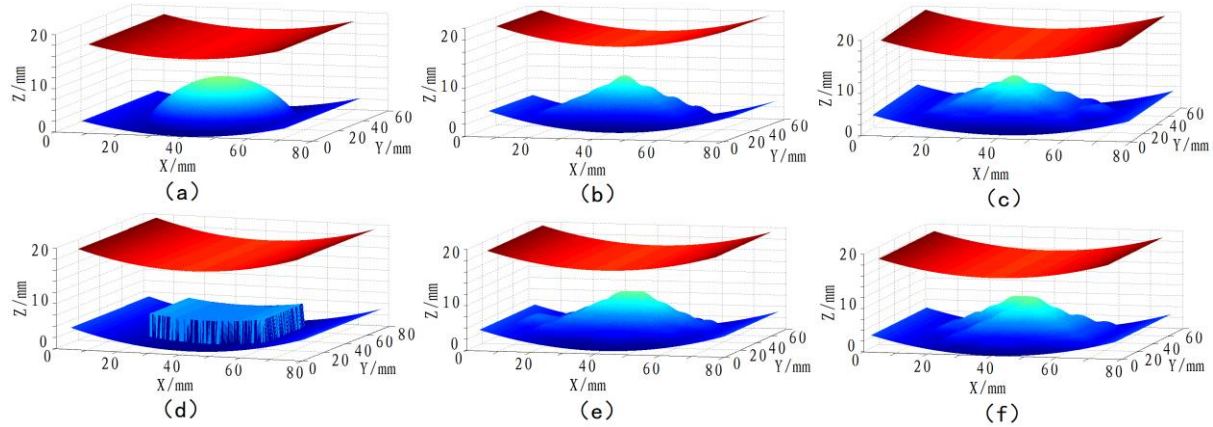

Fig. 10. Reconstruction of external globoid defect, 42.9 mm×7.15 mm: (a) real defect profile; (b), (c) reconstructed defects based on 3-D simulated and 1-D measured signals, using general GA with randomly generated initial population; (d) prediction result of NN inversion; (e), (f) reconstructed defects based on 3-D simulated and 1-D measured signals, using GA with initial solution from NN inversion.

Then the reconstruction is conducted again using the proposed hybrid inversion method, with the prediction of NN as one original solution of the GA inversion. The prediction results for the three defects from NN are shown in Fig. 8 (d), Fig. 9 (d) and Fig. 10 (d). Figure 8 (e), Fig. 9 (e), and Fig. 10 (e) depict the final predicted profiles of the three defects based on 3-D simulated MFL signals. Similarly, Fig. 8 (f), Fig. 9 (f), and Fig. 10 (f) show the predicted defect profiles based on 1-D measured MFL signals. Compared with former inversion results using general GA, reconstructed defects match the real ones better when prediction results of NN are used as the original solutions of the GA in the hybrid inversion procedure. In fact, the efficiency of defect reconstruction has been improved significantly, and the accuracy of reconstruction has increased within same time.

The reconstruction errors in different situations are then calculated and summarized as Table 2. The larger errors of reconstructed results using general GA with randomly generated original solutions demonstrate that the optimization fails to converge to the global minimum solution within fixed number of iterations. When the prediction of NN is used as original solution in the hybrid inversion procedure, the iterative GA could produce obviously better results of defect reconstruction.

To further testify the robustness of the proposed hybrid inversion procedure, a randomly generated internal defect as Fig. 11 (a) is simulated using the reduced forward model to get corresponding 3-D simulated MFL signals. The reconstructed defect profile using the proposed hybrid inversion procedure, based

on the basic 7×10×10 defect model shown in Fig. 5, is shown in Fig. 11 (b). Then the hybrid inversion procedure is conducted again, based on a refined 15×20×20 defect model, to get a new reconstructed defect profile (Fig. 11 (c)). The results of reconstruction show that the proposed hybrid inversion procedure is rather effective and robust even for randomly generated defect profile. Furthermore, the accuracy of reconstruction could get improved using a refined defect model extended from the basic one shown in Fig. 5.

Table 2: Reconstruction errors of different defects

Defect/mm	Simulated Signals		Measured Signals	
	General GA	Hybrid	General GA	Hybrid
Internal cuboid 100.1×14.3×5.7	0.12	0.05	0.21	0.14
External cuboid 42.9×42.9×8.6	0.13	0.05	0.22	0.15
External globoid 42.9×7.15	0.25	0.12	0.41	0.28

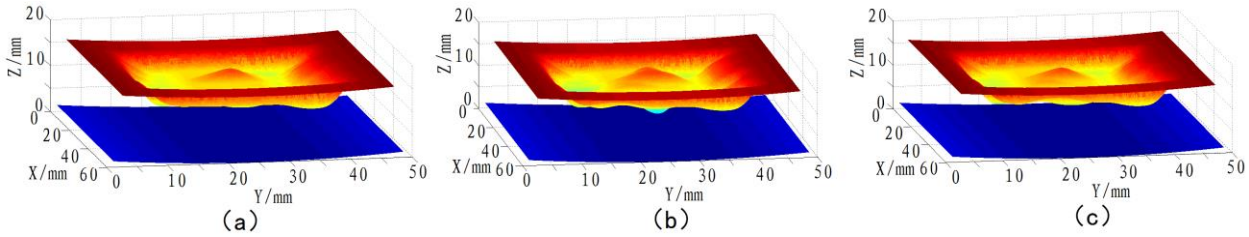

Fig. 11. Reconstruction of randomly generated defect using proposed hybrid inversion method based on 3-D simulated MFL signals: (a) real defect profile; (b) reconstructed defect using basic 7×10×10 defect model; (c) reconstructed defect using refined 15×20×20 defect model.

V. CONCLUSION

In this paper, a hybrid inversion approach is presented to reconstruct the 3-D defect profile from MFL signals in pipeline inspection. The reduced FE forward model of MFL inspection is developed, and the defect area is represented by an array of 7×10×10 partial cylinder cells. The NN is used at first to get a prediction of the defect, which is then utilized as one original solution of the GA to search for the global optimum estimate of the defect profile. Accuracy and efficiency of the proposed hybrid inversion method is demonstrated by the reconstruction results from both simulated and experimental MFL signals. Comparison between results from simulated and measured MFL signals also show that all the three components, instead of only the axial or radial component, of MFL signals in pipeline inspection should be detected for better reconstruction results. Furthermore, the accuracy of reconstruction could get improved using a refined defect model.

Future work will concentrate on optimizing the forward model to reduce time consumption and refining the defect model to increase accuracy of defect prediction. Besides, more kinds of defect shape should be covered in the experiment to test the proposed inversion method.

REFERENCES

[1] A. Khodayari-Rostamabad, J. P. Reilly, N. K. Nikolova, et al., "Machine learning techniques for the analysis of magnetic flux leakage images in pipeline inspection," *IEEE Transactions on Magnetics*, vol. 45, no. 8, pp. 3073-3084, 2009.

[2] M. Ravan, R. K. Amineh, S. Koziel, et al., "Sizing of 3-D arbitrary defects using magnetic flux leakage measurements," *IEEE Transactions on Magnetics*, vol. 46, no. 4, pp. 1024-1033, 2010.

[3] P. Ramuhalli, L. Udpa, and S. S. Udpa, "Electromagnetic NDE signal inversion by function-approximation neural networks," *IEEE Transactions on Magnetics*, vol. 38, no. 6, pp. 3633-3642, 2002.

[4] A. Joshi, "Wavelet transform and neural network based 3D defect characterization using magnetic flux leakage," *International Journal of Applied Electromagnetics and Mechanics*, vol. 28, no. 1, pp. 149-153, 2008.

[5] S. R. H. Hoole, S. Subramaniam, R. Saldanha, et al., "Inverse problem methodology and finite elements in the identification of cracks, sources, materials, and their geometry in inaccessible locations," *IEEE Transactions on Magnetics*, vol. 27, no. 3, pp. 3433-3443, 1991.

[6] R. Priewald, C. Magele, P. Ledger, et al., "Fast magnetic flux leakage signal inversion for the reconstruction of arbitrary defect profiles in steel using finite elements," *IEEE Transactions on Magnetics*, vol. 49, no. 1, pp. 506-516, 2013.

[7] K. C. Hari, M. Nabi, and S. V. Kulkarni, "Improved FEM model for defect-shape

construction from MFL signal by using genetic algorithm," *Science, Measurement & Technology, IET*, vol. 1, no. 4, pp. 196-200, 2007.

[8] M. Yan, S. Udpa, S. Mandayam, et al., "Solution of inverse problems in electromagnetic NDE using finite element methods," *IEEE Transactions on Magnetics*, vol. 34, no. 5, pp. 2924-2927, 1998.

[9] A. A. Adly and S. K. Abd-El-Hafiz, "Utilizing particle swarm optimization in the field computation of non-linear magnetic media," *ACES Journal*, vol. 18, no. 3, pp. 202-209, 2003.

[10] J. Chen, S. Huang, and W. Zhao, "Three-dimensional defect reconstruction from magnetic flux leakage signals in pipeline inspection based on a dynamic taboo search procedure," *Insight-Non-Destructive Testing and Condition Monitoring*, vol. 56, no. 10, pp. 535-540, 2014.

[11] P. S. Kildal and A. Kishk, "EM modeling of surfaces with STOP or GO characteristics-artificial magnetic conductors and soft and hard surfaces," *ACES Journal*, vol. 18, no. 1, pp. 32-40, 2003.

[12] M. M. Bibby and F. P. Andrew, "High accuracy calculation of the magnetic vector potential on surfaces," *ACES Journal*, vol. 18, no. 1, pp. 12-22, 2003.

Junjie Chen was born in 1988. He received his Ph.D. degree from Tsinghua University in 2015. He is currently working on problems in power system.